CRYSTAL GROWTH & DESIGN

Article

pubs.acs.org/crystal

Influence of the Hydroxyl Position in Racemic Hydroxyoctadecanoic Acids on the Crystallization Kinetics and Activation Energies of Gels and Dispersions in Mineral Oil

Michael A. Rogers,*[,†] Shibu Abraham,[‡] Ferenc Bodondics,[§] and Richard G. Weiss[‡]

[†]Department of Food Science, Rutgers University; The State University of New Jersey, New Brunswick, New Jersey 08901, United States

[‡]Department of Chemistry, Georgetown University, Washington, D.C. 20057-1227, United States

[§]Canadian Light Source, Saskatchewan, Saskatoon S7N0X4, Canada

ABSTRACT: Minor changes in molecular structure affect the ability of racemic hydroxyoctadecanoic acids (*n*HSA, where *n* is the position of the hydroxyl group) to form molecular gels in a low polarity liquid, mineral oil, and influence their supramolecular structures. The activation energy and energy released during crystallization of 2HSA and 3HSA from solutions or sols are significantly lower than those of 6HSA, 8HSA, 10HSA, 12HSA, and 14HSA. The lower activation energies are associated with the ease of molecules of 2HSA or 3HSA to add to a face of a growing crystal lattice or the ease in which the critical nuclei are reached; the change in the activation energies appears to be related, in part, to the critical size of the crystallites, which, in turn, depends on the energy associated with the creation of the new phase and the interfacial free energy of the nucleated species with the liquid component. When the polar groups are close in proximity, the crystal packing arrangements are able to sequester these groups away from an interface and reduce the contact with the low polarity solvent. As well, the energies released upon the formation of the new phases with 2HSA and 3HSA are less than those for the other *n*HSA isomers studied here because the former are unable to form strong carboxylic acid dimers.

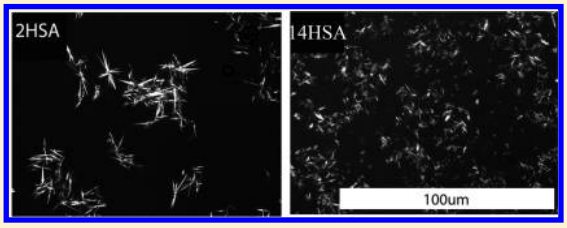

INTRODUCTION

Molecular organogels are thermally reversible, quasi-solid materials comprised mainly of an organic liquid (usually ≥95%) and a molecule that self-assembles noncovalently into a three-dimensional network of fibrillar objects (SAFiNs) or, less frequently, of platelets, nanotubes, etc.[1−3] The networks prevent macroscopic flow of the liquid and even can improve the mechanical properties of some solids.[4,5] The unique physical properties of SAFiNs have led to investigations focused on possible applications related to photovoltaics,[6] light harvesting,[7] templating reactions,[7] controlled drug release,[8] and reversible photoisomerizations.[9]

Self-assembly of molecular gels is an intricate and complex process that must balance contrasting parameters, including solubility and those intermolecular forces that control epitaxial growth into axially symmetric elongated aggregates.[2,10−13] During the assembly process, individual molecules assemble into oligomers driven by molecular self-recognition and intermolecular noncovalent interactions; subsequently, these oligomers assemble into fibril aggregates immobilizing the solvent via capillary forces.[14,15] In general, optimal gelation occurs when the solvent and gelator are unable to form intermolecular noncovalent bonds and the SAFiN is comprised of thin entangled fibers.[16] Typically, the intermolecular forces that drive aggregation include hydrogen-bonding,[17−20] $\pi-\pi$ stacking,[21] dipole−dipole,[22,23] and London dispersion forces;[24] however, hydrogen-bonding is a very important component of the self-assembly driving force in a large fraction of reported organogelators.[9,18,25]

On a molecular level, the required structural characteristics for self-assembly into molecular gels are not well understood. For instance, chiral and enantiopure 12-hydroxystearic acids (D-12HSAs) assemble into drastically different networks, one being platelets and the other fibrillar, respectively.[26−28] With minor molecular differences affecting the crystal physics, it is extremely important to understand how these physical interactions affect the formation of supramolecular architectures; they are the key to reaching rational design strategies for developing new classes of low molecular weight organogelators (LMOGs).

Here, we present an investigation of the molecular characteristics required to promote self-assembly and gelation within a group of positional isomers of racemic hydroxyoctadecanoic acid (*n*HSA, where *n* is the position of the hydroxyl group along the polymethylene chain). D-12HSA, a structurally simple, highly effective LMOG, has been studied extensively for gelation kinetics[18,29−31] and supramolecular structure formation,[19,32−36] as well as to monitor surface properties,[37] solvent polarity,[11,38] the influence of minor components,[39] and effects of chemical structure.[26,38,40−43] Within this report, we explore

Received: July 27, 2012
Revised: September 18, 2012

   dx.doi.org/10.1021/cg301071x | *Cryst. Growth Des.* XXXX, XXX, XXX−XXX

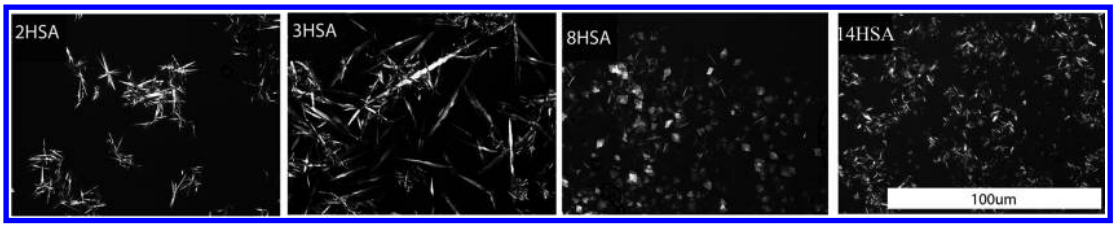

Figure 1. Polarized light micrographs of positional isomers of 2 wt % gels and dispersions of *n*HSA in mineral oil at 30 °C. The magnification bar applies to all panels.

how the gelating kinetics and crystallization activation energy are affected when the position of the hydroxyl group of *n*HSA is moved. The aim of this study is to identify factors that influence self-assembly and organogelation of a series of racemic *n*HSA in which the carboxyl headgroup is unchanged but the position of the hydroxyl group is moved along the alkyl chains.

EXPERIMENTAL SECTION

Materials. Light mineral oil (Aldrich), synthetic DL-2-hydroxystearic acid (Matreya, 98%), DL-3-hydroxystearic acid (Matreya, 98%), DL-6-hydroxystearic acid (Materya, 98%), D-12-hydroxysteaic acid (Aldrich, 99%), ethyl acetate (Fischer, HPLC grade), dichloromethane (Fischer, HPLC grade), tetradecanedioic acid (Aldrich, 99%), sebacic acid (Aldrich, 99%), suberic acid (Aldrich, ≥98%), cyclohexane (EMD chemicals, ACS grade, >99%), hexane (Aldrich, HPLC grade), ethanol (The Warner-Graham Company, 190 proof, 95%), ethanol (Aldrich, anhydrous), $NaHCO_3$ (Aldrich, ReagentPlus, ≥99.5%), KOH (Aldrich, ACS reagent, >85%), and conc. hydrochloric acid (EMD chemicals, 36.5−38%) were used as received. Syntheses of the other positional isomers of hydroxyoctadecanoic acids employed here were reported by Abraham et al.[44]

A mixture of an *n*HSA in mineral oil was heated to 110 °C and held there for 20 min (to ensure loss of "crystal history"). The melting temperatures of the neat *n*HSA and their gels/dispersions were based on differential scanning calorimetry measurements. Unless stated otherwise, the *n*HSA concentrations were 2.0 wt %.

Instrumentation. A Nikon Eclipse E400 light microscope equipped with a Nikon DS-FiL color camera and a long working distance 10× lens and condenser (Nikon Instruments Inc., Melville, NY, USA) were used to acquire polarized light micrographs. A temperature-controlled stage (LTS120 and PE94 temperature controller; Linkam, Surrey, U.K.) was used to control the crystallization temperature of the solutions/sols that were varied from 10 to 35 °C in 5 °C intervals. The image resolution was 2560 by 1920 pixels. Samples were prepared by adding a drop of the melted sample onto a glass microscope slide, and a 25 mm × 25 mm coverslip was applied.

Fourier transform infrared spectroscopy (FT-IR) spectra were collected using the end station of the mid-IR beamline (beamline 01B1-01) of the Canadian Light Source, Saskatoon, SK. The end station is comprised of a Bruker Optics IFS66v/S interferometer coupled to a Hyperion 2000 IR microscope (Bruker Optics, Billerica, MA, USA). A drop of sample was placed between two 2 mm thick, 25 mm diameter, CaF_2 disks separated by a 15 μm Teflon spacer. Light was focused on it using a 15× magnification Schwarzschild condenser, collected by a 15× magnification Schwarzschild objective with the aperture set to a spot size of 40 μm by 40 μm and detected by a liquid nitrogen-cooled narrow-band MCT detector utilizing a 100 μm sensing element.

A KBr-supported Ge multilayer beam splitter was used to measure spectra in the mid-infrared spectral region using molten hydroxyoctadecanoic acid in mineral oil as the background. Measurements were performed using OPUS 6.5 software (Bruker Optics, Billerica, MA). The measured interferograms were an average of 32 scans and were recorded by scanning the moving mirror at 40 kHz (in relation to the reference HeNe laser wavelength of 632.8 nm). Scans from 690 to 7899 cm^{-1} with a spectral resolution of 4 cm^{-1} were recorded every 10 s. Single-channel traces were obtained using the fast Fourier transform algorithm without any zero-filling, after applying a Blackman-Harris three-term apodization function.

Ten to twelve milligrams of 2% *n*HSA in mineral oil was placed in Alod-Al hermetic DSC pans and heated to 100 °C and then subsequently cooled at 2 °C/min to 10 °C and held there for 10 min using a Q2000 differential scanning calorimeter (DSC) (TA Instruments, New Castle, DE). Following the temperature hold, the samples were heated to 120 °C at 2 °C/min while the chamber was continually flushed with nitrogen (0.5 mL/min), and the melting temperature, melting enthalpy, crystallization temperature, and crystallization enthalpy were calculated by integrating the peak area using the sigmodal baseline integration technique, which is part of the TA Instruments analysis software package. Each sample was run in triplicate.

RESULTS AND DISCUSSION

At 2.0 wt % of 6HSA, 8HSA, 10HSA, 12HSA, or 14HSA in mineral oil, molecular gels form allowing the glass vials in which they were placed to be inverted without detectable flow.[44] However, 2HSA and 3HSA did not immobilize the mineral oil and exhibited properties similar to a viscous solution. Under polarized light (Figure 1), the 2HSA and 3HSA crystal morphologies differ dramatically from those of the other *n*HSA capable of self-assembling into molecular gels (i.e., 6HSA, 8HSA, 10HSA, 12HSA, and 14HSA).

2HSA and 3HSA mineral oil dispersions have few nucleated sites and the supramolecular structure develops mainly via radial crystal growth, occurring in a fibril fashion from nucleating centers (Figure 2). Very little interpenetration of the crystal domains is observed; neither continuous crystal networks nor organogels are formed. When the hydroxyl group is at or beyond position 6 on the fatty acid backbone, the resulting crystals are orthorhombic platelets (Figure 1). These HSAs have many more individual crystals, indicating that more nucleating sites form during the initial stages of SAFiN growth and less subsequent crystal growth. The large number of small platelets interpenetrate, forming a three-dimensional network capable of entrapping the liquid component. The presence of platelets for these systems is expected because the synthesis occurs from the reduction of a keto group, which is not stereoselective: previous work has shown that DL-12HSA results in platelets, whereas D- or L-12HSA provide fibers.[26,41]

In an attempt to quantify the microstructure, the individual nuclei on polarized light micrographs were counted as a function of area and the longest crystal axis was measured using Image J software (Figure 2). As can be seen in Figure 3A, the number of nucleation sites differs drastically depending on the position of the hydroxyl group. For 2HSA and 3HSA, the number of crystals on a micrograph (approximate area 125 μm × 125 μm) is between 50 and 75. As the position of the hydroxyl group is moved farther from the carboxylic acid moiety, the number of nucleation sites steadily increases until it

dx.doi.org/10.1021/cg301071x | Cryst. Growth Des. XXXX, XXX, XXX−XXX

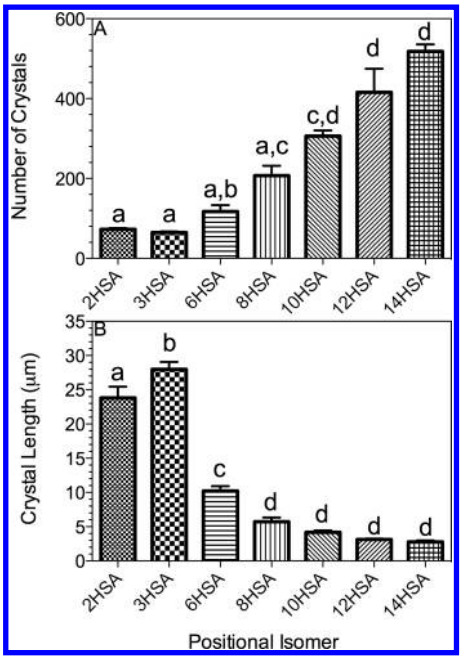

Figure 2. Number of nuclei (A) and length of fibers (B) obtained from polarized light micrographs.

exceeds 500. Conversely and as expected, as the number of distinct crystals increases, the crystal length decreases (Figure 2B). There is a distinct drop in the crystal size corresponding to the large increase in the number of crystals when the position of the hydroxyl group is moved beyond carbon 6. Previously, it was found that the X-ray diffractograms of the *n*HSAs with $n \geq 6$ have diffraction peaks representative of both long and short spacings while 2HSA and 3HSA only have a long spacing.[44] Although what drives this difference in molecular packing is still not clear, it must be related to the possible motions of the aliphatic chains of the molecules.

Assembly of individual *n*HSA molecules into fibril aggregates is an exothermic process. The amount of heat per gram of gelator released during the self-assembly of *n*HSA in mineral oil depends on the energy of the new noncovalent interactions.[33,44] The fibril crystals formed by 2HSA and 3HSA have a lower corresponding energy than those of 6HSA though 14HSA (Figure 3A). The lower energy associated with the transition from sol to dispersion of 2HSA and 3HSA is consistent with the lack of their formation of cyclic carboxylic acid dimers and the inability of their secondary hydroxyl groups to interact efficiently.[44] The transition temperatures for 2HSA and 3HSA dispersions are higher than for the positional isomers that form organogels (Figure 3B).

Crystallization temperature (T) and crystallization enthalpy (ΔH) have been used to calculate the change in the entropy ($\Delta S = \Delta H/T$) (Figure 3C) during the sol-to-gel/dispersion transitions that are reversible. A similar trend to that of the ΔH was observed in the ΔS changes as a function of n: the entropies of 2HSA and 3HSA are significantly lower than those of the 8−14HSA isomers. This difference is associated with the polar carboxylic acid head groups and secondary hydroxyl groups of 2HSA and 3HSA being in proximity on the molecules. Such a molecular arrangement allows the polar head groups to be more effectively shielded from the low polarity solvent, mineral oil, in the sol. Hence the 6−14HSAs have stronger interactions between the low-polarity solvent and the polar entities of the molecules. Furthermore, the lower ΔS for 2HSA and 3HSA are consistent with the smaller number of distinct peaks observed in their X-ray diffractograms[44] and suggest again greater conformational freedom for these fatty acid chains compared with those of the other *n*HSA examined.

The difference between the crystallization and melting temperatures was used to calculate the degree of undercooling

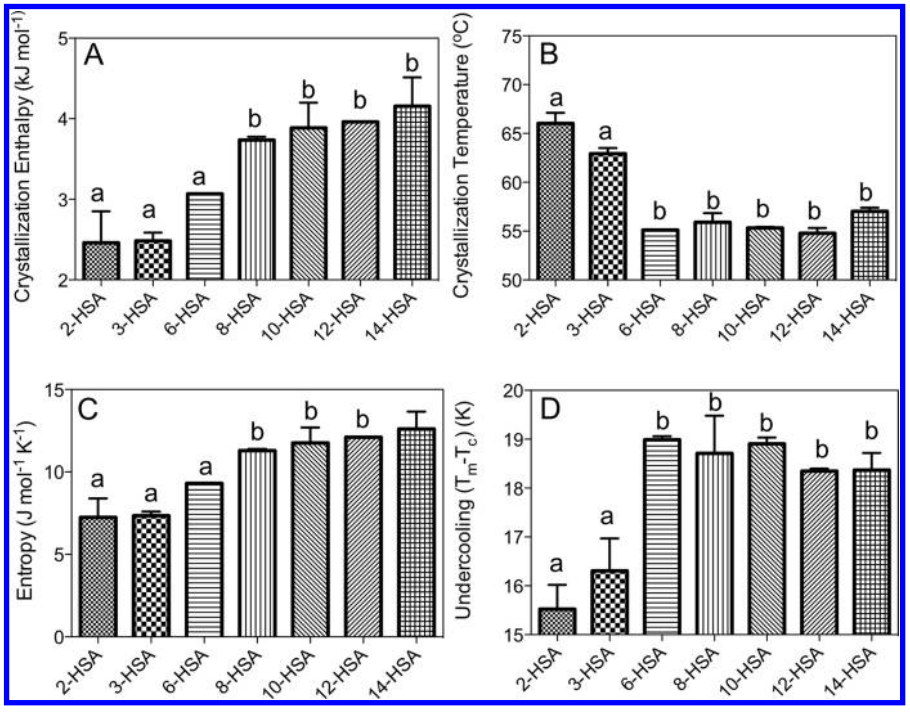

Figure 3. Crystallization enthalpy (A), temperature, (B) entropy (C), and degree of undercooling (D) for the positional isomers of *n*HSA−mineral oil gels from differential scanning calorimetry. Adapted in part from ref 44.

dx.doi.org/10.1021/cg301071x | *Cryst. Growth Des.* XXXX, XXX, XXX−XXX

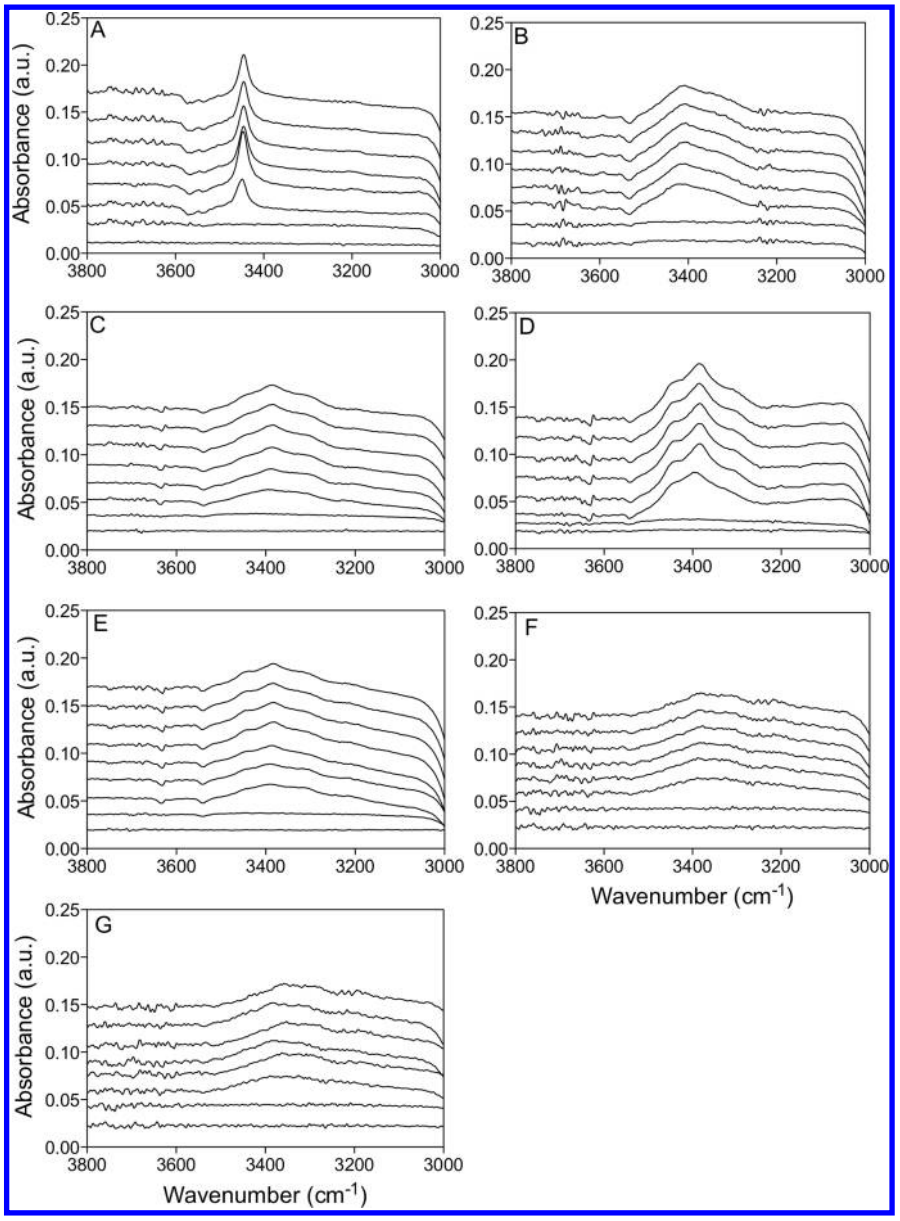

Figure 4. Vertically offset FT-IR spectra focusing on the hydroxyl region, using the molten sol as the background, for the mineral oil gels of 2HSA (A), 3HSA (B), 6HSA (C), 8HSA (D), 10HSA (E), 12HSA (F), and 14HSA (G) quench cooled to 30 °C. Spectra were collected every 10 s, and the time between displayed spectra is 1 min.

(Figure 3D). The degree of undercooling for 2HSA and 3HSA is approximately 4 °C lower than for the *n*HSA molecules that form organogels. The lower degree of under cooling suggests that when the *n*HSA have a high polarity end and a low polarity end, the molecules more easily phase separate to form a critical nucleus. Classical crystal theory states that a phase change, such as crystallization, occurs when the overall free energy, ΔG, goes from positive to negative or at the instant that $\Delta G = 0$. In the case of a spherical cluster, eq 1 holds at the transition temperature when $\Delta G = 0$.

$$\Delta G = -\frac{4}{3}\pi r^3 G_v + 4\pi r^2 \sigma \tag{1}$$

Then, the embryonic critical radius, r^*, is given by eq 2 where G_v is the energy released during the formation of the crystal phase and σ is the free energy associated with the formation of a new surface from a spherical cluster with radius r.

$$r^* = -\frac{2\sigma}{G_v} \tag{2}$$

Therefore, there are two components that affect the early stages of nucleation: the interfacial free energy and the energy associated with the new phase (i.e., the enthalpy released during the assembly/crystallization process). As the hydroxyl group is moved farther from the carboxylic acid moiety, we hypothesize that the aliphatic nature of the molecule may make it more difficult to phase separate because the interfacial free energy of the new phase is higher, thus resulting in a larger critical radius because the hydrophilic components are more difficult to exclude from the solid−liquid interface. Another possible explanation is that the energy for the new noncovalent interactions for 6−14HSA is greater than for 2HSA and 3HSA. Previous work supports molecular interactions being much stronger for 6HSA, 8HSA, 10HSA, 12HSA, and 14HSA (which are capable of forming very strong cyclic carboxylic

dx.doi.org/10.1021/cg301071x | *Cryst. Growth Des.* XXXX, XXX, XXX−XXX

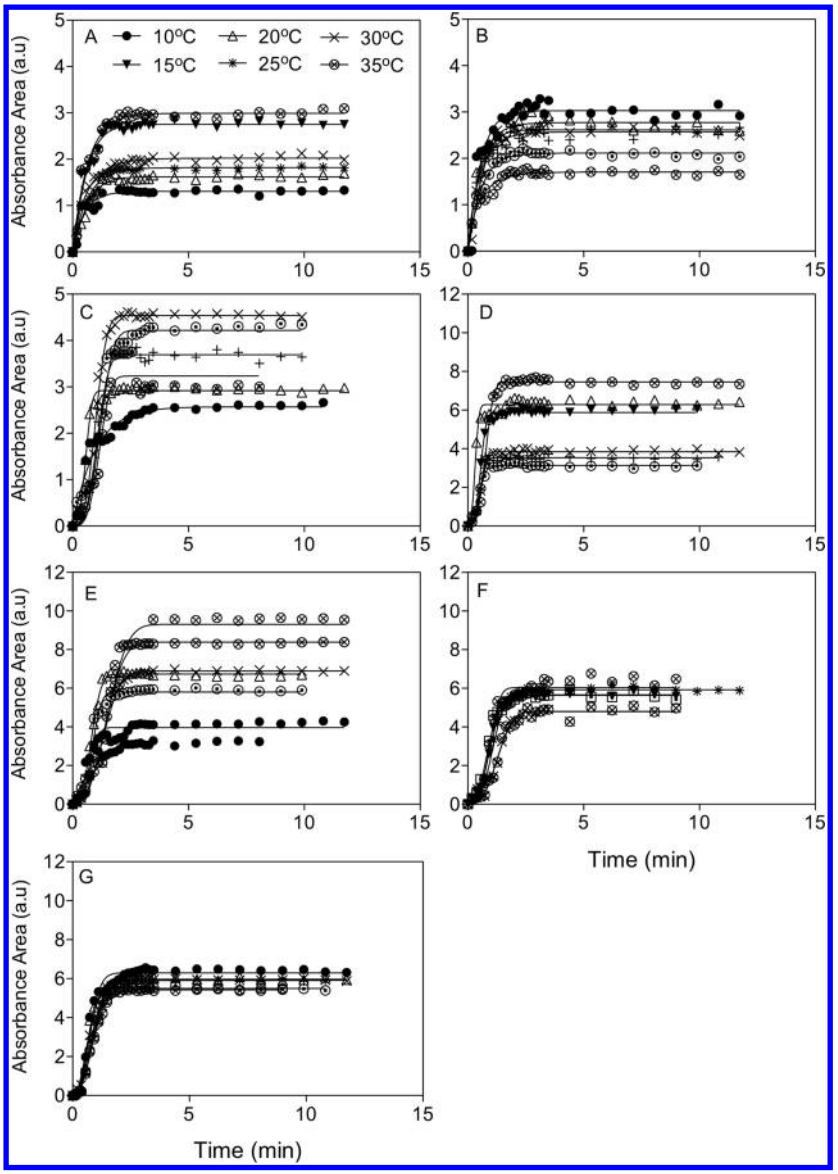

Figure 5. Integration of the FT-IR signal at 3450 cm^{-1} for the mineral oil gels of 2HSA (A), 3HSA (B), 6HSA (C), 8HSA (D), 10HSA (E), 12HSA (F), and 14HSA (G) at 10, 15, 20, 25, 30, and 35 °C.

dimers) than for 2HSA and 3HSA (which form only acyclic carboxylic dimers or remain monomeric). This observation is also supported by the difference in energy released during crystallization (Figure 3A). If this hypothesis is correct, differences should be observed in the activation energy for crystallization, and there are.

Previously, we have shown that the relative increase in the area of the IR peak at 3200 cm^{-1}, corresponding to nonspecific hydrogen bonding that occurs during self-assembly, correlates well with the increase in the volume of the new crystal phase (Figure 4).[18,26,31] Here, spectra were collected every 10 s for each crystallization temperature and integrated to determine the peak areas between 3200 and 3600 cm^{-1} (Figure 5). The sigmoidal curves observed for the self-assembly process were fitted to the Avrami equation (eq 3) where Y is the phase volume (i.e., the area under the peak), k is the reaction rate constant, x is time, and n is the Avrami exponent.[45−47]

$$Y = 1 - e^{-k(x)^n} \quad (3)$$

The Avrami exponent is a measure of the type of nucleation (i.e., sporadic or instantaneous) and dimensionality of crystal growth. It typically has an integer or half-integer value between 1 and 4.[48] For example, an Avrami exponent of 1 corresponds to instantaneous nucleation and linear crystal growth, while an exponent of 2 may correspond to either sporadic nucleation and linear growth or instantaneous nucleation and platelet-like growth.[31] Upon fitting the Avrami equation to the sigmoidal curves, the Avrami exponent for 2HSA and 3HSA was calculated to be 1, while for 6−14HSA, the value was 3. From this data treatment, we conclude that 2HSA and 3HSA undergo instantaneous nucleation and linear growth; the mode of crystal growth is confirmed by the polarized light micrographs (Figure 1). On the other hand, 6−14HSA undergo either sporadic nucleation and platelet-like growth or instantaneous nucleation and spherulitic growth. It is obvious, from the polarized light micrographs that a platelet crystal morphology is present and, therefore, nucleation must be sporadic. A possible explanation for the difference in the modes of nucleation is that instantaneous nucleation is favored over

dx.doi.org/10.1021/cg301071x | Cryst. Growth Des. XXXX, XXX, XXX−XXX

sporadic nucleation when the free energy of nucleation is lower.[48] This explanation seems to be supported by the nucleation component of the Avrami exponent (Figure 6A).

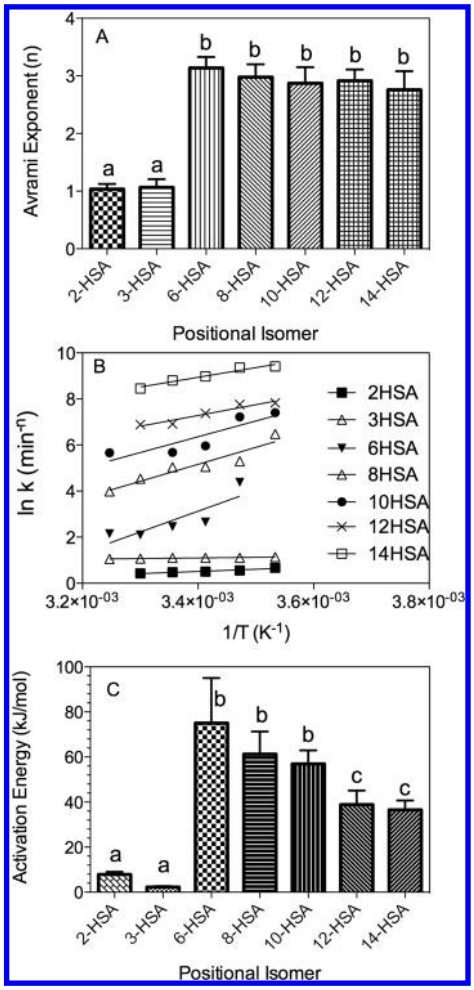

Figure 6. Avrami exponent (A) and rate constants (B) calculated by fitting Figure 4 to the Avrami equation and the activation energy (C) calculated using an Arrhenius model of the rate constants determined for the positional isomers of *n*HSA−mineral oil gels. Bars represent one standard error.

Furthermore, if the free energy barrier is lower, as in the cases of 2HSA and 3HSA, the degree of undercooling (Figure 3D) should also be lower than those of 6−14HSA. To determine whether this is the case, the rate constants determined at different crystallization temperatures were plotted in Figure 6B using the Arrhenius model (eq 4) where ln A is the frequency factor, E_a is the activation energy, R is the ideal gas constant, and T is the crystallization temperature.

$$\ln k = \ln A + \frac{E_a}{RT} \tag{4}$$

The activation energy may only be calculated in this fashion if the dimensionality of growth, n, is the same at each incubation temperature (as it is here). A linear regression between ln k and the inverse of temperature yielded a correlation coefficient, R_2, values greater than 0.89 for all fits (Figure 6B). Interestingly, the calculated activation energies for nucleation were lower for fiber formation than for platelet formation. The activation energy, a measure of the rate-limiting step, may be related to the ease of phase separation in the sol state, the ability of gelator molecules to accrete onto the early nuclei surface, or the ability of a gelator molecule to adapt the ideal molecular conformation to add to a crystal face. The decision to form platelets or fibers must be made at the early stages of phase separation, nucleation, or growth. Both 2HSA and 3HSA have activation energies below 10 kJ/mol, while the remaining HSAs have activation energies between 40 and 80 kJ/mol. It is obvious from the mode of nucleation (Figure 6A) and the activation energy (Figure 6C) that minor changes in the molecular structure affect nucleation and crystallization at the earliest stages, which most likely occur at or around the formation of the subcritical nucleated species.

CONCLUSIONS

Minor structural changes to hydroxyoctadecanoic acids, effected by altering the position of the hydroxyl group along the polymethylene chain, cause enormous changes in the SAFiNs of the molecular gels and dispersions formed by these molecules in mineral oil, a low-polarity, high-viscosity liquid. The *n*HSAs have two polar entities, which when placed near each other (i.e., as in 2HSAand 3HSA) result in the activation energy and energy of crystallization of the dispersions being much lower than when the two groups are separated by ≥5 carbon atoms (i.e., as in 6−14HSA). The reduced activation energy may be associated with the ease with which the molecules incorporate into the growing crystal lattice or the ease with which the critical nucleus is reach. Probably, a combination of these factors is responsible because the critical radius is a balance between the energy associated with creating a new phase and the interfacial free energy of the new surface. Hence, when the two polar groups are close, the crystal arrangement is able to remove these groups from the liquid interface and reduce the contact with the low polarity solvent. Also, the energy of the new phase is lower for 2HSA and 3HSA because of their inability to form strong carboxylic acid dimers.

AUTHOR INFORMATION

Corresponding Author

*E-mail: rogers@AESOP.Rutgers.edu.

Notes

The authors declare no competing financial interest.

ACKNOWLEDGMENTS

The research described in this paper was performed at the Canadian Light Source, which is supported by NSERC, NRC, CIHR, and the University of Saskatchewan. The authors are grateful to Tim May (CLS) for beamline design and construction and for constant help in beamline upkeep. This project was supported by the HATCH Program through the New Jersey Agriculture Research Station (NJAES). S.A. and R.G.W. thank the US National Science Foundation for its support of the research performed at Georgetown.

REFERENCES

(1) Mallia, V. A.; et al. Reversible Phase Transitions within Self-Assembled Fibrillar Networks of (R)-18-(n-Alkylamino)octadecan-7-ols in Their Carbon Tetrachloride Gels. *J. Am. Chem. Soc.* **2011**, *133*, 15045−15054.

(2) Weiss, R. G.; Terech, P. Introduction. In *Molecular Gels: Materials with Self-Assebled Fibrillar Networks*; Weiss, R. G., Terech, P., Eds.; Springer: Dordrecht, The Netherlands, 2006; pp 1−13.

(3) George, M.; Weiss, R. G. Molecular Organogels. Soft Matter Comprised of Low-Molecular-Mass Organic Gelators and Organic Liquids. *Acc. Chem. Res.* **2006**, *39*, 489−497.
(4) Fahrländer, M.; et al. Linear and Nonlinear Rheological Properties of Self-Assembling Tectons in Polypropylene Matrices. *Macromolecules* **2003**, *36*, 3749−3757.
(5) Isare, B.; et al. The Weak Help the Strong: Low-Molar-Mass Organogelators Harden Bitumen. *Langmuir* **2009**, *25*, 8400−8403.
(6) Kubo, W.; et al. Quasi-Solid-State Dye-Sensitized TiO_2 Solar Cells: Effective Charge Transport in Mesoporous Space Filled with Gel Electrolytes Containing Iodide and Iodine. *J. Phys. Chem. B* **2001**, *105*, 12809−12815.
(7) Sugiyasu, K.; Fujita, N.; Shinkai, S. Visible-Light-Harvesting Organogel Composed of Cholesterol-Based Perylene Derivatives. *Angew. Chem., Int. Ed.* **2004**, *43*, 1229−1233.
(8) Friggeri, A.; Feringa, B. L.; van Esch, J. Entrapment and release of quinoline derivatives using a hydrogel of a low molecular weight gelator. *J. Controlled Release* **2004**, *97*, 241−248.
(9) Wu, Y.; et al. Solvent effects on structure, photoresponse and speed of gelation of a dicholesterol-linked azobenzene organogel. *Soft Matter* **2011**, *7*, 9177−9183.
(10) Suzuki, M.; et al. Effects of hydrogen bonding and van der Waals interactions on organogelation using designed low-molecular-weight gelators and gel formation at room temperature. *Langmuir* **2003**, *19* (21), 8622−8624.
(11) Rogers, M. A.; Marangoni, A. G. Solvent-Modulated Nucleation and Crystallization Kinetics of 12-Hydroxystearic Acid: A Non-isothermal Approach. *Langmuir* **2009**, *25* (15), 8556−8566.
(12) Raynal, M.; Bouteiller, L. Organogel Formation Rationalized by Hansen Solubility Parameters. *Chem. Commun.* **2011**, *47*, 8271−8273.
(13) Gao, J.; Wu, S.; Rogers, M. A. Harnessing Hansen Solubility Parameters to Predict Organogel Formation. *J. Mater. Chem.* **2012**, *22*, 12651−12658.
(14) Hardy, J. G.; Hirst, A. R.; Smith, D. K. Exploring molecular recognition pathways in one- and two-component gels formed by dendritic lysine-based gelators. *Soft Matter* **2012**, *8*, 3399−3406.
(15) Edwards, W.; Lagadec, C. A.; Smith, D. K. Solvent-gelator interactions–using empirical solvent parameters to better understand the self-assembly of gel-phase materials. *Soft Matter* **2011**, *7*, 110−117.
(16) Zhu, G.; Dordick, J. S. *Solvent Effect on Organogel Formation by Low Molecular Weight Molecules* **2006**, *18* (Chemistry of Materials), 5988−5995.
(17) Kuwahara, T.; et al. Crystal structure of DL-12-hydroxystearic acid. *Chem. Lett.* **1996**, *25*, 435−436.
(18) Lam, R.; et al. A molecular insight into the nature of crystallographic mismatches in self-assembled fibrillar networks under non-isothermal crystallization conditions. *Soft Matter* **2010**, *6* (2), 404−408.
(19) Li, J. L.; et al. Arichitecture of a Biocompatible Supramolecular Material by Supersaturation-Driven Fabrication of its Network. *J. Phys. Chem. B* **2005**, *109*, 24231−24235.
(20) Rogers, M. A.; et al. Multicomponent Hollow Tubules Formeed Using Phytosterol and γ-Oryzanol-Based Compounds: An Understanding of Their Molecular Embrace. *J. Phys. Chem. A* **2010**, *114*, 8278−8295.
(21) Moffat, J. R.; Smith, D. K. Controlled Self-Sorting in the Assembly of 'Multi-Gelator' Gels. *Chem. Commun.* **2009**, *3*, 316−318.
(22) Brotin, T.; Devergne, J. P.; Fages, F. Photostationary Fluorescence Emission and Time Resoved Spectroscopy of Symmetrically Disubstituted Anthracenes on teh meso and Side Rings: The Unusual Behavior of the 1,4 Derivative. *Photochem. Photobiol.* **1992**, *55*, 349−358.
(23) Terech, P.; Furman, I.; Weiss, R. G. Structures of Organogels Based Upon Cholesteryl 4-(2-Anthryloxy)Butanoate, A Highly Efficient Luminescing Gelator - Neutron and X-Ray Small-Angle Scattering Investigations. *J. Phys. Chem.* **1995**, *99* (23), 9558−9566.
(24) Toro-Vazquez, J. F.; et al. Relationship Between Molecular Structure and Thermo-mechanical Properties of Candelilla Wax and Amides Derived from (*R*)-12-Hydroxystearic Acid as Gelators of Safflower Oil. *Food Biophys.* **2010**, *5* (3), 193−202.
(25) van Esch, J.; Feringa, B. L. New functional materials based on self-assembling organogels: From serendipity towards design. *Angew. Chem., Int. Ed.* **2000**, *39*, 2263−2266.
(26) Grahame, D. A. S.; et al. Influence of Chirality on the Modes of Self-Assembly of 12-Hydroxystearic Acid in Molecular Gels of Mineral Oil. *Soft Matter* **2011**, *7*, 7359−7365.
(27) Tachibana, T.; Kambara, H. Sense of twist in fibrous aggregates from 12-hydroxystearic acid and its alkali metal soaps. *J. Colloid Interface Sci.* **1968**, *28* (1), 173−178.
(28) Tachibana, T.; Mori, T.; Hori, K. Chiral Mesophases of 12-Hydroxyoctadecanoic Acid in Jelly and in the Solid State. I. A New Type of Lyotropic Mesophase in Jelly with Organic Solvents. *Bull. Chem. Soc. Jpn.* **1980**, *53*, 1714−1719.
(29) Terech, P. Kinetics of Aggregation in a Steroid Derivative/Cyclohexane Gelifying System. *J. Colloid Interface Sci.* **1985**, *107* (1), 244−255.
(30) Rogers, M. A.; Marangoni, A. G. Non-Isothermal Nucleation and Crystallization of 12-Hydroxystearic Acid in Vegetable Oils. *Cryst. Growth Des.* **2008**, *8* (12), 4596−4601.
(31) Lam, R. S. H.; Rogers, M. A. Experimental Validation of the Modified Avrami Model for Non-Isothermal Crystallization Conditions. *CrystEngComm* **2010**, *13*, 866−875.
(32) Li, J. L.; et al. Nanoengineering of a Biocompatible Organogel by Thermal Processing. *J. Phys. Chem. B* **2009**, *113* (15), 5011−5015.
(33) Rogers, M. A.; Wright, A. J.; Marangoni, A. G. Engineering the oil binding capacity and crystallinity of self-assembled fibrillar networks of 12-hydroxystearic acid in edible oils. *Soft Matter* **2008**, *4* (7), 1483−1490.
(34) Rogers, M. A.; Wright, A. J.; Marangoni, A. G. Nanostructuring fiber morphology and solvent inclusions in 12-hydroxystearic acid/canola oil organogels. *Curr. Opin. Colloid Interface Sci.* **2009**, *14* (3), 223−223.
(35) Rogers, M. A.; Wright, A. J.; Marangoni, A. G. Nanostructuring fiber morphology and solvent inclusions in 12-hydroxystearic acid/canola oil organogels. *Curr. Opin. Colloid Interface Sci.* **2009**, *14* (1), 33−42.
(36) Wang, R. Y.; et al. Architecture of Fiber Network: From Understanding to Engineering of Molecular Gels. *J. Phys. Chem. B* **2006**, *10*, 25797−25802.
(37) Menger, F. M.; et al. Chain-Substituted Lipids in Monomolecular Films. Effect of Polar Substituents on Molecular Packing. *Langmuir* **1989**, *5*, 833−838.
(38) Mallia, V. A.; et al. Robust Organogels from Nitrogen-Containing Derivatives of (*R*)-12-Hydroxystearic Acid as Gelators: Comparisons with Gels from Stearic Acid Derivatives. *Langmuir* **2009**, *25* (15), 8615−8625.
(39) Fameau, A. L.; et al. 12-Hydroxystearic acid lipid tubes under various experimental conditions. *J. Colloid Interface Sci.* **2010**, *341* (1), 38−47.
(40) Huang, X.; Weiss, R. G. Molecular organogels of the sodium salt of (*R*)-12-hydroxystearic acid and their templated syntheses of inorganic oxides. *Tetrahedron* **2007**, *63* (31), 7375−7385.
(41) Sakurai, T.; et al. A Comparative Study on Chiral and Racemic 12-Hydroxyoctadecanoic Acids in the Slutions and Aggregation States: Does the Racemic Form Really Form a Gel? *Bull. Chem. Soc. Jpn.* **2010**, *83* (2), 145−149.
(42) Terech, P.; et al. Organogels and Areogels of Racemic and Chiral 12-Hydroxyoctadecanoic Acid. *Langmuir* **1994**, *10* (10), 3406−3418.
(43) Wright, A. J.; Marangoni, A. G. Time, temperature, and concentration dependence of ricinelaidic acid-canola oil organogelation. *J. Am. Oil Chem. Soc.* **2007**, *84* (1), 3−9.
(44) Abraham, S.; et al. Influence of Positional Isomers on the Macroscale and Nanoscale Architectures of Aggregates of Racemic Hydroxyoctadecanoic Acids in Their Molecular Gel, Dispersion, and Solid States. *Langmuir* **2012**, *28*, 4955−4964.

(45) Avrami, M. Kinetics of Phase Change. I. General Theory. *J. Chem. Phys.* **1939**, *7* (12), 1103−1112.
(46) Avrami, M. Kinetics of Phase Change. II. Transformation-Time Relations for Random Distribution of Nuclei. *J. Chem. Phys.* **1940**, *8* (22), 212−226.
(47) Avrami, M. Kinetics of Phase Change. III. Granulation, Phase Change, and Microstructure. *J. Chem. Phys.* **1941**, *9* (2), 177−184.
(48) Marangoni, A. G. Crystallization Kinetics. In *Fat Crystal Networks*; Marangoni, A. G., Ed.; Marcel Dekker: New York, 2005; pp 21−82.